BIOCHEMISTRY
including biophysical chemistry & molecular biology

Article

pubs.acs.org/biochemistry

Identification and Co-complex Structure of a New *S. pyogenes* SpeB Small Molecule Inhibitor

Ana Y. Wang, Gonzalo E. González-Páez, and Dennis W. Wolan*

Departments of Molecular and Experimental Medicine and Chemical Physiology, The Scripps Research Institute, 10550 N. Torrey Pines Road, La Jolla, California 92037, United States

Supporting Information

ABSTRACT: The secreted *Streptococcus pyogenes* cysteine protease SpeB is implicated in host immune system evasion and bacterial virulence. We present a small molecule inhibitor of SpeB **2477** identified from a high-throughput screen based on the hydrolysis of a fluorogenic peptide substrate Ac-AIK-AMC. **2477** inhibits other SpeB-related proteases but not human caspase-3, suggesting that the molecule targets proteases with the papain-like structural fold. A 1.59 Å X-ray crystal structure of **2477** bound to the SpeB active site reveals the mechanism of inhibition and the essential constituents of **2477** necessary for binding. An assessment against a panel of **2477** derivatives confirms our structural findings and shows that a carbamate and nitrile on **2477** are required for SpeB inhibition, as these moieties provide an extensive network of electrostatic and hydrogen-bonding interactions with SpeB active site residues. Surprisingly, despite **2477** having a reduced inhibitory potential against papain, the majority of **2477**-related compounds inhibit papain to a much greater and broader extent than SpeB. These findings indicate that SpeB is more stringently selective than papain for this panel of small molecule inhibitors. On the basis of our structural and biochemical characterization, we propose modifications to **2477** for subsequent rounds of inhibitor design that will impart specificity to SpeB over other papain-like proteases, including alterations of the compound to exploit the differences in CA protease active site pocket sizes and electrostatics.

Streptococcal pyrogenic exotoxin B (SpeB) is a cysteine protease of the papain-fold protease family (clan CA)[1] secreted by the majority of *Streptococcus pyogenes* strains, a Gram-positive bacterium that only infects humans.[2] *S. pyogenes* infections lead to many ailments, such as tonsillitis, scarlet fever, and meningitis. Deep penetration into tissues by the bacterium can lead to more serious diseases, including necrotizing fasciitis and sepsis.[3] Currently, there are no *S. pyogenes*-specific treatments for infection, and high mortality rates are associated with invasive infections. Therefore, the development of new therapies and approaches toward combating these infections is needed.

Many factors produced by *S. pyogenes* have been implicated in establishing and disseminating infection. Primarily, studies focused on the production and secretion of SpeB have suggested SpeB proteolytic activity promotes *S. pyogenes* pathogenicity through the cleavage of biologically relevant substrates involved in host immune evasion, including immunoglobulin A (IgA), IgE, and properdin as well as inflammation, such as interleukin-1β (IL-1β) and H-kininogen.[4−6] Likewise, SpeB degradation of host extracellular matrix proteins fibronectin and vitronectin and tight-junction proteins E-cadherin and occludin compromises human tissue integrity and promotes infiltration of *S. pyogenes*.[7,8] SpeB activity also releases streptococcal cell surface proteins proposed to enhance *S. pyogenes* infectivity.[9] Importantly, the spatial and temporal consequences that specific degradation and/or activation of human and bacterial substrates by SpeB with respect to *S. pyogenes* infectivity have yet to be resolved.

Recent studies question the contribution of SpeB to *S. pyogenes* virulence. For example, down-regulation of SpeB by genetic methods (e.g., allelic exchange mutagenesis) or inhibition of proteolysis by the covalent, clan CA inhibitor *trans*-epoxysuccinyl-L-leucylamido(4-guanidino)butane (E64) has shown that increased SpeB activity promotes lesion development in infected tissues, spread of infection, and biofilm formation.[10,11] On the contrary, group A *Streptococcus* (GAS) strains with mutations in the SpeB expression regulator CovS that decrease or eliminate SpeB show that the absence of SpeB activity leads to the accumulation of activated host protease plasmin. This increased level of active plasmin is suggested to enhance *S. pyogenes* pathogenicity through the direct cleavage of bacterial surface proteins required for infectivity.[12,13]

As an alternative to genetic approaches, several peptide-based clan CA inhibitors have been developed. These amino acid-containing inhibitors encompass both reversible (i.e., aldehydes, α-diketones, α-ketoesters, α-ketoamides, and α-ketoacids) and irreversible (i.e., peptidyl diazomethyl ketones, fluoromethyl ketones, epoxides, and vinyl sulfones) warhead functionalities at

Received: January 9, 2015
Revised: June 29, 2015
Published: July 1, 2015

DOI: 10.1021/acs.biochem.5b00607
Biochemistry 2015, 54, 4365−4373

the C-terminus.[14,15] Not surprisingly, these peptide inhibitors promiscuously inhibit SpeB, papain, and other related proteases, as the clan CA protease specificities are focused to a subset of amino acid recognition sequences.[16,17] Therefore, the chemical space diversity to develop protease-specific peptide inhibitors with amino acid constituents is limited.

Another approach to find specific and selective inhibitors toward an individual protease among the highly conserved clan CA is through the discovery and development of small molecules. There is an increased likelihood to design and tailor protease-specific synthetic inhibitors, as small molecule design can sample a much larger chemical space than peptides and can be designed to be independent of highly conserved peptide recognition motifs among the active sites of clan CA proteases. Small molecules also have more attractive physical properties than peptides for therapeutic development, including improved potential for membrane permeability and resistance to protease degradation during host administration.[18,19]

Small molecule-based SpeB inhibitors have yet to be described. As such, we sought to identify SpeB inhibitors and use these validated compounds as chemical tools to ultimately probe the importance of SpeB to *S. pyogenes* pathogenicity. Application of a new class of SpeB inhibitors would address the necessity of this protease to *S. pyogenes* within cellular and animal infection models, as well as establish SpeB as a target for the development of treatments to combat streptococcal infections.

From a high-throughput screen (HTS) of SpeB inhibition, we identified small molecule **2477** as a reversible inhibitor of SpeB activity. We determined a high-resolution cocrystal structure of **2477** in the active site of SpeB and further validated the **2477** binding motifs by exploring the inhibition of SpeB by a panel of **2477** derivatives. Our *in vitro* kinetic analyses demonstrate that a carbamate and nitrile of **2477** are necessary for effective SpeB inhibition. We also show that papain, despite a decreased affinity for **2477**, is more susceptible to inhibition by **2477** analogues, indicating a more stringent selectivity of SpeB for this family of inhibitors. Comparison of SpeB and papain reveals that the electrostatic landscape and size of the papain active site accounts for inhibitor promiscuity. Such differences in active site architecture also provide insight into the future design and development of small molecules that preferentially inhibit SpeB over other clan CA protease members.

MATERIALS AND METHODS

SpeB Preparation and Purification. The *S. pyogenes* 10782 zymogen SpeB clone (residues 28−398) was overexpressed and purified as a C-terminal His_6-tag fusion (additional amino acids for the affinity tag include LEH_6, residues 399−406) from *E. coli* BL21DE3pLysS (Strategene) in a pET23b vector (Novagen), as previously described.[20] Mature SpeB was concentrated to approximately 10 mg/mL using Millipore Ultrafree-15 devices with a MWCO of 3500 Da and immediately stored at −80 °C. The C-terminal His_6-tag was not removed from the SpeB protein preparations, as the presence of the tag does not interfere with *in vitro* kinetics and is positioned on the opposite side of the protein surface more than 50 Å from the active site. All components of the assay were stored as frozen aliquots and thawed immediately prior to the assay.

SpeB High-Throughput Screen. We synthesized and measured SpeB activity with an N-terminal acetylated, fluorogenic SpeB tripeptide substrate acetyl-Ala-Ile-Lys-7-aminomethylcoumarin (Ac-AIK-AMC) based on previously determined optimal cleavage sequences.[21] This substrate synthesis was previously described using standard Fmoc solid phase synthesis chemistry starting with Fmoc-Lys(carbamate)-AMC Wang resin (EMD Biosciences).[20] The HTS SpeB inhibitor assay protocol was modified based on optimized fluorescence that resulted from cleavage of Ac-AIK-AMC (Figure 1A) by 50 nM active SpeB in an activity buffer

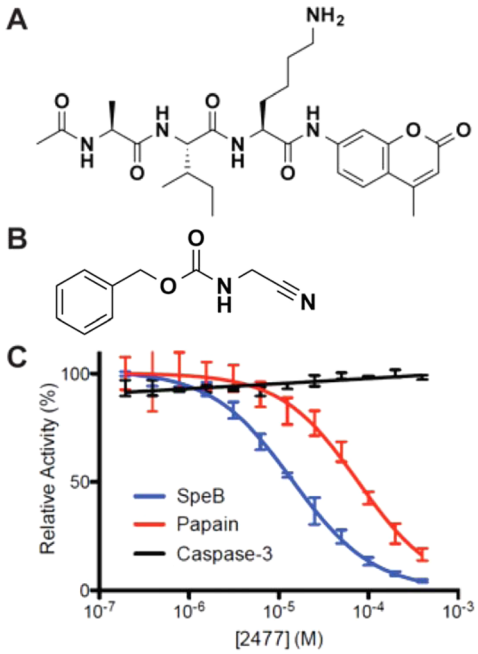

Figure 1. Identification and characterization of SpeB inhibitor **2477**. (A) Structure of fluorogenic SpeB substrate Ac-AIK-AMC. (B) Structure of inhibitor **2477**. (C) **2477** IC_{50} curves with SpeB, papain, and caspase-3.

consisting of PBS at pH 7.4, 0.1 mM EDTA, 10 mM DTT, and 0.1% CHAPS. 100 nM SpeB diluted in activity buffer was incubated in low-volume, 384-well plates with a final concentration of 15 μM Maybridge HitFinder HTS compound library compounds in a volume of 10 μL (0.5% DMSO). Following 30 min of incubation at 25 °C, 10 μL of 50 μM Ac-AIK-AMC was subsequently added to the SpeB mixture and incubated for an additional 30 min at 25 °C (final concentration of 50 nM SpeB and 25 μM Ac-AIK-AMC). Fluorescence intensity due to AMC hydrolysis was measured on a PerkinElmer EnVision plate reader (excitation 355 nm, emission 460 nm). We incorporated the DMSO vehicle and 15 μM of the general proteinase inhibitor E64 as the negative and positive controls, respectively. The completed assay included 50 screened plates (16,000 compounds) with an average Z′ of 0.88, an overall signal-over-background of 15×, and a hit rate of 0.018% (3× standard deviation over the mean).

SpeB and Papain Kinetic Assays and IC_{50} Determination. SpeB was incubated at 50 nM in the presence of increasing amounts of inhibitor (3 μM to 200 μM) in a reaction buffer consisting of PBS at pH 7.4, 0.1 mM EDTA, 10 mM DTT, and 0.1% CHAPS and incubated for 30 min at 25 °C. Fifty micromolar Ac-AIK-AMC was subsequently added, and the rate of substrate hydrolysis was measured by increase in fluorescence every 20 s for a 5 min duration in 96-well plates on

DOI: 10.1021/acs.biochem.5b00607
Biochemistry 2015, 54, 4365−4373

a PerkinElmer EnVision plate reader. Michaelis–Menten (K_i) and IC_{50} values were determined using GraphPad Prism software (GraphPad, Inc.).

Caspase-3 Kinetic Assays. Ten nanomolar caspase-3 was incubated in the presence of **2477** (3 μM to 200 μM) in a buffer consisting of 50 mM HEPES at pH 7.4, 0.1% CHAPS, 10 mM KCl, 50 mM sucrose, 1 mM $MgCl_2$, and 10 mM DTT and incubated at 25 °C for 30 min. Fifty micromolar Ac-DEVD-AFC was then added, and the rate of substrate hydrolysis was measured by increase in fluorescence every 10 s for 2 min in a 96-well microtiter plate on a PerkinElmer EnVision plate reader with excitation at 355 nm and emission detection at 486 nm, as previously described.[22] The velocity of substrate turnover was analyzed using GraphPad Prism software.

Crystallization and X-ray Data Collection. Crystals of mature SpeB in complex with **2477** were grown by sitting drop-vapor diffusion, as previously described.[20] Briefly, inhibitor **2477** was added in 2-fold molar excess to SpeB and incubated for 2 h at 25 °C and immediately used for cocrystallization experiments. Crystals of SpeB in complex with **2477** were grown from a solution consisting of 0.15 M sodium nitrate with 22% PEG 3500 at 25 °C by mixing equal volumes (2 μL) of SpeB (10 mg/mL) and the reservoir solution. The His_6-tag was not removed as the protein crystallized readily.

Data for the SpeB X-ray structure in complex with **2477** were collected on single, flash-cooled crystals at 100 K in a cryoprotectant consisting of mother liquor and 20% PEG 400 and were processed with HKL2000 in orthorhombic space group $P2_12_12$ (Table 1).[23] The calculated Matthews' coefficient (V_M = 1.95 Å^3 Da^{-1}) suggested one monomer per asymmetric unit with a solvent content of 37%. X-ray data for the **2477**-SpeB structure were collected to 1.59 Å resolution on beamline 11.1 at the Stanford Synchrotron Radiation Lightsource (SSRL) (Menlo Park, CA). Data collection and processing statistics are summarized in Table 1.

Structure Solution and Refinement. The **2477**-SpeB complex structure was determined by molecular replacement (MR) with Phaser[24,25] using the previously published mature apo SpeB structure (PDB ID 4D8B)[20] as the initial search model. All structures were manually built with Coot[26] and iteratively refined using Phenix[27] with cycles of conventional positional refinement. TLS B-factor refinement was carried out in the last 3 rounds of refinement with the SpeB monomer split into 8 TLS groups as determined by TLS Motion Determination in Phenix. TLS refinement resulted in improved electron density maps with a minimal change in R_{cryst} and R_{free}. The electron density maps clearly identified that inhibitor **2477** was located within the SpeB active site. Water molecules were automatically positioned by Phenix using a 2.5σ cutoff in $F_o - F_c$ maps and manually inspected. A nitrate molecule from the buffer bound to residues located within the C-terminal loop. The final R_{cryst} and R_{free} are 16.1% and 18.8%, respectively (Table 1).

All models were analyzed and validated with PROCHECK,[25,28] WHATCHECK,[29] and Molprobity[30] on the Joint Center for Structural Genomics (JCSG) Web server. Analysis of backbone dihedral angles with the program PROCHECK indicated that all residues for the three structures are located in the most favorable and allowed regions in the Ramachandran plot with no outliers. Coordinates and structure factors have been deposited in the PDB,[31] with accession entry 4RKX. Structure refinement statistics are shown in Table 1.

Table 1. SpeB-2477 Co-complex X-ray Data Processing and Structure Refinement Statistics

structure	SpeB-**2477**
PDB ID	4RKX
space group	$P2_12_12$
unit cell parameters (a, b, c) (Å)	114.56, 50.36, 37.41
unit cell angles (z, y, z)	90.0, 90.0, 90.0
Data Processing	
resolution range (Å) (outer shell)	50–1.59 (1.64–1.59)
unique reflections	26,926 (2,327)
completeness (%)	89.6 (86.5)
redundancy	3.4 (3.3)
R_{meas} (%)[a]	8.9 (30.3)
R_{merge} (%)[b]	7.6 (26.0)
$R_{p.i.m.}$ (%)[c]	4.5 (15.2)
average I/average $\sigma(I)$	11.0 (3.6)
Refinement	
resolution range (Å)	31.3–1.59 (1.65–1.59)
no. of reflections[d] (test set)	26,810 (2,426)
R_{cryst} (%)[e]	16.1 (20.3)
R_{free} (%)[e]	18.8 (25.9)
protein atoms/waters	1953/206
CV[f] coordinate error (Å)	0.14
RMSD bonds (Å)/angles (deg)	0.005/0.93
B-values protein/waters/ligands (Å^2)	17.8/28.5/29.4
Ramachandran Statistics (%)	
most favored	98.4
additional allowed	1.6
generously allowed	0

[a] $R_{meas} = \{\Sigma_{hkl}[N/(N-1)]1/2\Sigma_i|I_{i(hkl)} - \langle I_{(hkl)}\rangle|\}/\Sigma_{hkl}\Sigma_i I_{i(hkl)}$, where $I_{i(hkl)}$ is the observed intensity, $\langle I_{(hkl)}\rangle$ is the average intensity, and N is the multiplicity of reflection hkl. [b] $R_{merge} = \Sigma_{hkl}\Sigma_i|I_{i(hkl)} - \langle I_{(hkl)}\rangle|/\Sigma_{hkl}S_iI_{i(hkl)}$ where $I_{i(hkl)}$ is the i^{th} measurement of reflection h and $\langle I\rangle$ is the average measurement value. [c] $R_{p.i.m.}$ (precision-indicating R_{merge}) = $S_{hkl}[1(N_{hkl}-1)]^{1/2}S_i|I_{i(hkl)} - \langle I_{(hkl)}\rangle|/S_{hkl}S_iI_{i(hkl)}$. [d] Reflections with $I > 0$ were used for refinement.[32−34] [e] $R_{cryst} = \Sigma_h||F_{obs}| - |F_{calc}||/\Sigma|F_{obs}|$, where F_{obs} and F_{calc} are the calculated and observed structure factor amplitudes, respectively. R_{free} is R_{cryst} with 5.0% test set structure factors. [f] Cross-validated (CV) Luzzati coordinate errors.

RESULTS

We designed and executed an *in vitro* HTS assay using hydrolysis of a fluorogenic tripeptide substrate Ac-AIK-AMC as a readout to search for SpeB inhibitors (Figure 1A). We based the SpeB substrate on previously reported optimal peptide cleavage sequences of SpeB.[31,32] Briefly, 100 nM SpeB was incubated with a 15 μM Maybridge HitFinder HTS compound library for 30 min at room temperature. Ac-AIK-AMC was subsequently added to a final concentration of 50 μM and measured for fluorescence intensity due to AMC cleavage after an additional 30 min incubation. We screened approximately 16,000 compounds for SpeB inhibition, and the assay was well behaved, as evidenced by a Z′ of 0.88 and a hit rate of 0.018%. We identified compound **2477** that resulted in approximately 22% inhibition under these stringent conditions and confirmed the molecule with follow-up assays (Figure 1B).

Compound **2477** is a reversible and competitive inhibitor of SpeB. An initial analysis revealed that SpeB is not covalently modified by **2477** as determined by subjecting the SpeB-**2477** complex to electrospray ionization mass spectrometry. The inhibitory potential of **2477** was tested on SpeB as well as the related papaya proteinase I or papain. Both proteases belong to

DOI: 10.1021/acs.biochem.5b00607
Biochemistry 2015, 54, 4365–4373

the clan CA, which contains families of cysteine peptidases structurally conserved with papain. The papain-like fold consists of an α-helix bundle and a β-barrel that surround an active site. The active site of these proteases has catalytic cysteine and histidine residues as well as an oxyanion hole to stabilize the substrate oxyanion transition state.[1]

SpeB and papain cleave substrate Ac-AIK-AMC with similar affinities (K_M of 216 μM and 248 μM, respectively); however, the catalytic efficiency of SpeB is significantly better than that of papain due to the substrate turnover (k_{cat} of 0.98 s^{-1} $\pm$ 0.10 and 0.53 s^{-1} $\pm$ 0.06, respectively) (Figure S1, Supporting Information). The **2477** IC_{50} values were determined for SpeB and papain by measuring the initial velocities of Ac-AIK-AMC hydrolysis after a 30-min incubation with increasing concentrations of **2477**. Similarly, the K_i values were assessed by measuring the initial velocities of substrate turnover while systematically varying the concentrations of substrate and inhibitor. We found that **2477** inhibits SpeB activity with an IC_{50} of 15 μM and K_i of 8 μM, and papain is inhibited to a lesser extent (IC_{50} of 72 μM and K_i of 45 μM) (Figure 1C, Figures S2 and S3, Supporting Information, and Table 2).

Table 2. K_i and IC_{50} Values of 2477 with SpeB and Papain

protease	K_i (μM)	IC_{50} (μM)
SpeB	8 $\pm$ 0.4	14 $\pm$ 1
papain	45 $\pm$ 2	77 $\pm$ 1

These results support **2477** as a general inhibitor of papain-like proteases and suggest the molecule will likely inhibit other closely related proteases within the CA clan, including staphopain A and calpain II. We next expanded the protease panel to include the structurally divergent human cysteine protease caspase-3. Caspase-3 activity was unaltered by the presence of **2477** (>400 μM) as determined by hydrolysis of the fluorogenic peptide substrate acetyl-Asp-Glu-Val-Asp-7-amino-trifluoromethylcoumarin (Ac-DEVD-AFC) at 50 μM (Figure 1C).

We determined the X-ray crystal structure of SpeB in complex with **2477** to elucidate the mechanism of small molecule inhibition (Figure 2A). The mature form of SpeB (residues 146–398 with a C-terminal His_6-tag) was incubated with a 2-fold molar excess of compound **2477** for 2 h at 25 °C in PBS at pH 7.0, with 1 mM DTT, and crystals were grown by mixing with an equal volume of 0.15 M sodium nitrate with 22% PEG 3500. The **2477**-bound SpeB structure is conserved

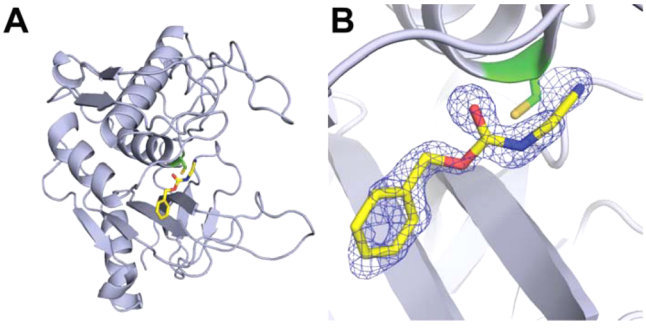

Figure 2. Crystal structure of **2477** bound within the SpeB active site. (A) Overall structure of SpeB with the location of **2477**. (B) **2477** modeled into the blue naïve $F_o - F_c$ electron density map contoured at 2σ.

with our previous apo and complex structures with crystallization in orthorhombic space group $P2_12_12$, an ordered leucine residue from the C-terminal His_6-tag (LEH_6), 245 water molecules, and a bound nitrate likely introduced from the crystallization buffer.[31] The apo SpeB structure (PDB ID 4D8B)[20] served as the initial search model for molecular replacement, and the initial $F_o - F_c$ electron density map exhibited unambiguous electron density for **2477** located within the SpeB active site (Figure 2B). The final R_{cryst} and R_{free} for the SpeB and **2477** co-complex crystal structure were 16.1% and 18.8%, respectively, with greater than 98% of residues in the favored region of the Ramachandran plot (Table 1). Compound **2477** was refined with 100% occupancy and has *B*-values similar to those of adjacent SpeB active site residues. The overall conformation of SpeB with **2477** is nearly identical to that of SpeB in complex with Ac-AEIK-CHO (PDB ID 4D8I),[20] as is evidenced by an RMSD of 0.14 Å for all Cα atoms with a maximum deviation of 0.62 Å.[34]

The **2477** carbonyl oxygen is oriented toward the SpeB oxyanion hole created by the main-chain nitrogen atoms of residues Cys192 and Val193 (Figures 3A and 4A). Importantly,

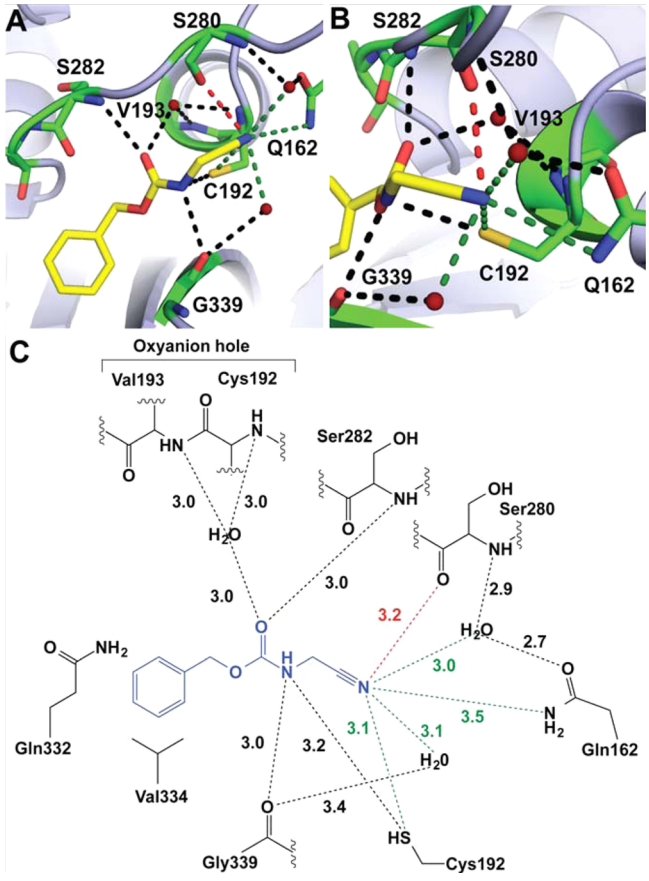

Figure 3. Crystal structure of SpeB active site interactions with **2477**. Atoms within hydrogen bonding distance of **2477** are shown with dashed lines. Red dashes include van der Waals repulsions within bonding distance. Green dashes indicate interactions that may be optimized through iterative alterations of **2477**. Waters are represented as red spheres. (A) Potential electrostatic interactions between the entire **2477** molecule with active site residues. (B) Potential electrostatic interactions between the carbamate nitrogen and nitrile of **2477** with surrounding residues. (C) Schematic of SpeB active site and **2477** interactions with bond distances.

DOI: 10.1021/acs.biochem.5b00607
Biochemistry 2015, 54, 4365–4373

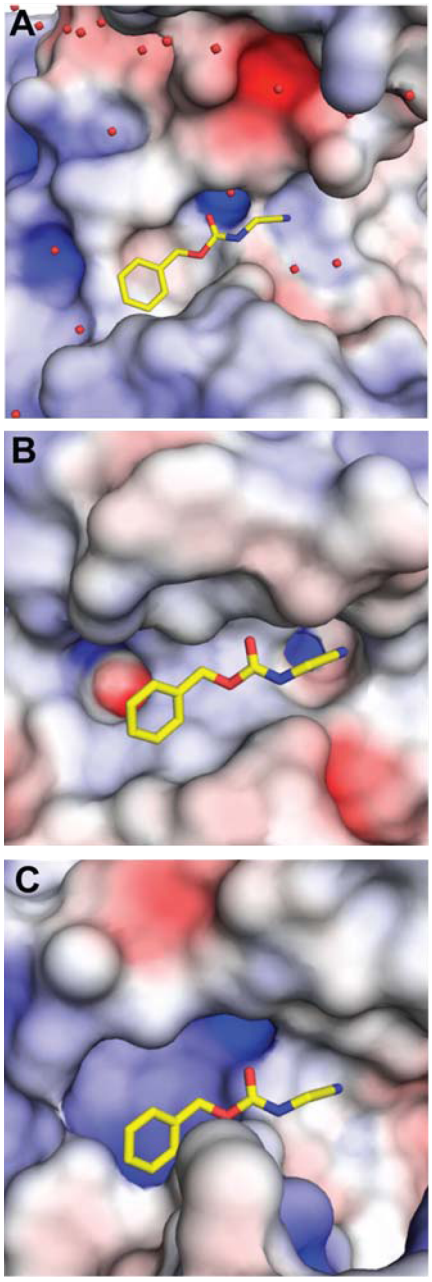

Figure 4. Electrostatic surface potentials of protease active sites bound to **2477**. Blue, positive potential (≥5 mV); white, neutral potential (0 mV); and red, negative potential (≤5 mV). (A) SpeB electrostatic surface potential shows alignment of the carbonyl oxygen with the oxyanion hole of the active site. (B) **2477** superimposed in the electrostatic surface map of the papain active site map shows the carbonyl oxygen of **2477** in a hydrophobic region. (C) **2477** superimposed in the electrostatic surface map of the staphopain A active site suggests effective binding of **2477**.

this interaction with the oxyanion hole is coordinated via a highly ordered water molecule positioned by Cys192 and Val193. The **2477** carbonyl is further stabilized by the main-chain carbamate nitrogen of Ser282. The main-chain oxygen atom of residue Gly339 and the thiol side chain of Cys192 act as hydrogen bond acceptors to the carbamate nitrogen of **2477**. The **2477** nitrile amine is within hydrogen-bonding distance to several active site residues and waters (Figure 3B,C); however, the geometric constraint of the nitrile triple bond limits potential interactions to coaxial hydrogen bonds. Two active site water molecules within hydrogen bonding distance of the nitrile are coordinated by the side chains of Gln162 and C192 and the main-chain carbonyl oxygen of Ser280. These potential interactions are highlighted by green dashes in Figure 3.

We analyzed SpeB and papain inhibition against a panel of **2477**-related compounds to gain an understanding of the essential features of **2477** that promote SpeB inhibition. All compounds tested (**1**−**11**) are shown in Figure S4, Supporting Information. We first addressed the importance of the nitrile group of **2477** by removing this moiety in **2** and **6** (Figure 5A). Not surprisingly, due to the number of active site interactions observed in the crystal structure with the nitrile moiety (Figure 3), **2** and **6** have no inhibitory potential against both SpeB and papain (Figure 5B,C). We next explored the importance of the **2477** phenyl ring by substitution with a large, hydrophobic *tert*-butyl group (**3**, Figure 5 and Figure S4, Supporting Information). We also tested the effect of adding steric bulk to the carbamate nitrogen with **4** (Figure S4, Supporting Information). The majority of compounds **1**−**6** showed poor inhibition of both SpeB and papain. Inhibition of SpeB was observed with **2**, **3**, and **6** at the highest concentrations assessed and were marginally effective in comparison to that of the other compounds (Figure 5B and Figures S5 and S6, Supporting Information). Similarly, papain inhibition was observed with **3** and **6** at the highest dosed concentrations (Figure 5C and Figure S6, Supporting Information).

Compounds **7**−**11** replaced the **2477** carbamate with a range of benzamide-containing compounds that retained the **2477** carbamate nitrogen and nitrile group but modified the phenyl ring with a variety of substitutions (Figure 5A and Figure S4, Supporting Information). The first compound in the benzamide series (**7**) was used to address how large of a hydrophic group could be accommodated by SpeB and papain (Figure 5A). Compound **7** is an established kinase inhibitor Momelotinib that is used as an ATP-competitive JAK 1/2 selective inhibitor.[35] Despite conservation of the major contributors of the electrostatic and hydrogen bonding carbamate and nitrile, the SpeB active site cannot accommodate the large bulky region of Momelotinib; however, it retains inhibition of papain as evidenced by the IC_{50} of 22 μM (Figure 5C). Compound **8** features a methyl and nitro group *ortho* and *meta* with respect to the carbamate, respectively, and retains some level of SpeB inhibition (IC_{50} >100 μM), likely due to the favorable electrostatic interactions between the negatively charged nitro group and the electropositive active-site pocket of SpeB (Figures 4A and 5B). Compound **8** inhibited papain with an IC_{50} lower than that of **2477** (18 μM) (Figure 5C). Addition of an *ortho* methyl ether and *para* methyl thioether onto the benzamide (**11**, Figure 5A) eliminated all ability to inhibit SpeB but retained some ability to accommodate the papain active site as evidenced by an IC_{50} >100 μM (Figure 5B,C).

DISCUSSION

Compound **2477** is a competitive inhibitor of SpeB as best evidenced by our crystal structure showing that the molecule binds within the SpeB active site (Figure 2A). Residues within the SpeB active site are positioned to provide several key potential hydrogen bonds and a hydrophobic pocket that direct binding **2477**. The phenyl ring of **2477** is nestled into a predominantly uncharged surface area composed of nonpolar residues Gly339, Val334, and Ala283. Despite primarily

DOI: 10.1021/acs.biochem.5b00607
Biochemistry 2015, 54, 4365−4373

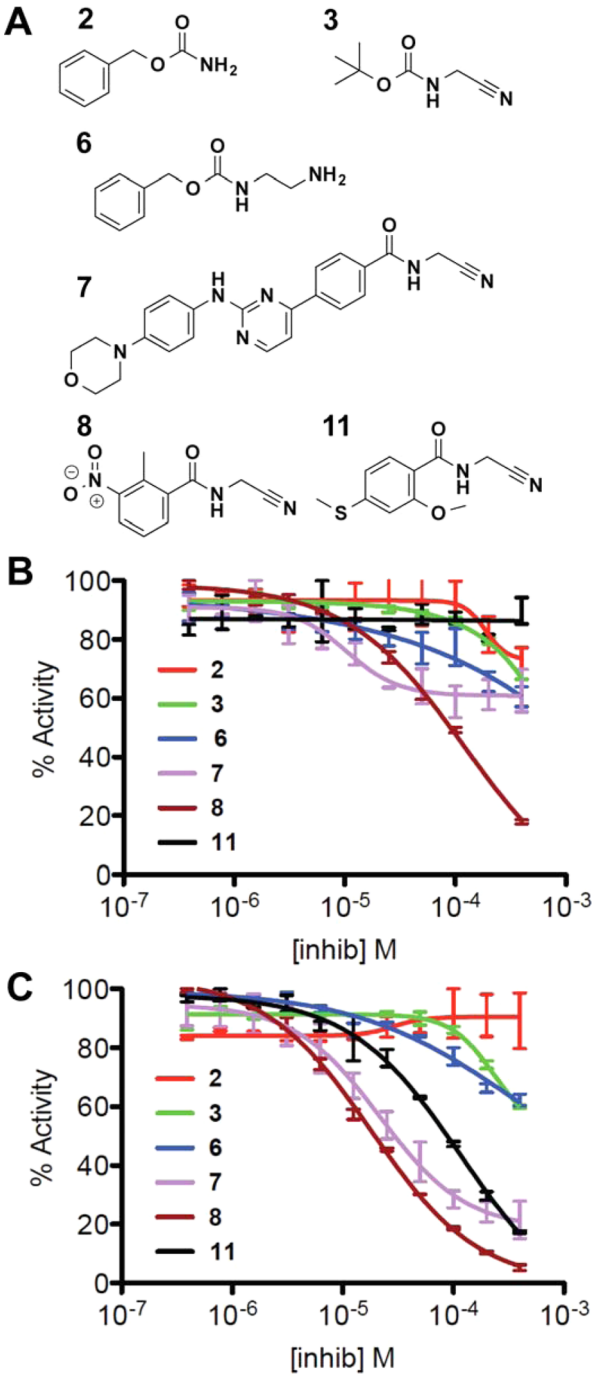

Figure 5. Assessment of **2477** derivatives for the inhibition potential of SpeB and papain. (A) Schematic structures of several compounds from the **2477** analogue library. IC_{50} assays of selected compounds against SpeB (B) and papain (C) performed in triplicate.

employing hydrophobicity and nonspecific main-chain hydrogen bonds, the active site of SpeB is fairly selective for the composition of **2477**, as analogues of the molecule did not inhibit the protease (Figure 5B).

Papain-like protease substrates generally prefer a basic residue in the P1 position (i.e., Lys or Arg) and a hydrophobic residue at P2.[21] On the basis of the X-ray structure, we find that significant interactions between SpeB and **2477** include hydrophobic effects and hydrogen bonds with nonspecific main-chain moieties. Therefore, **2477** is likely promiscuous toward the inhibition of homologous proteases, including papain and *Staphylococcus aureus* staphopain A, which is a C47 protease of clan CA.[1] Superposition of SpeB (PDB ID 4D8B),[20] papain (PDB ID 9PAP),[36] and staphopain A (PDB ID 1CV8)[37] X-ray structures reveal highly conserved secondary structures among the protease active sites (Figure 6), with

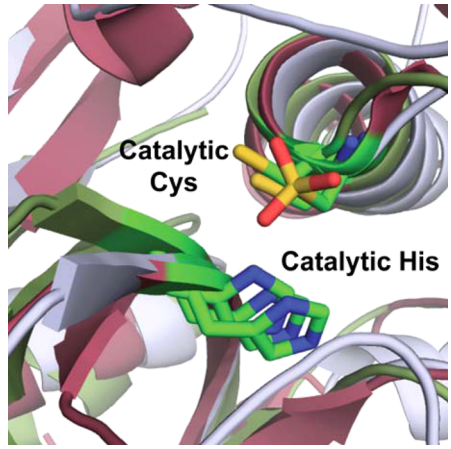

Figure 6. Superposition of active sites of SpeB (blue, PDB ID 4D8B), papain (red, PDB ID 9PAP), and staphopain A (green, PDB ID 1CV8) show high secondary structure conservation of active sites, including overlapping catalytic cysteine and histidine residues.

overlapping catalytic cysteine (shown as cysteinesulfonic acid in papain) and histidine residues. RMSD values for the overlaid structures are 1.94 Å between SpeB and papain (55 Cα atoms), and 1.50 Å between SpeB and staphopain A (59 Cα atoms). Surprisingly, despite the highly similar architecture of these protease active sites, our kinetic studies of **2477** analogues show that differences in amino acid residues between papain and SpeB impart unique affinities of the proteases for this family of molecules.

Superposition of **2477** into the active sites of papain and staphopain A suggests that the small molecule inhibits these proteases with interactions similar to that of SpeB. The phenyl ring of **2477** is located in a hydrophobic pocket of both papain (residues Val132, Val133, Gly78, and Gly79) and SpeB (Figure 4A,B). However, in staphopain A, the **2477** phenyl-binding pocket is more hydrophilic, as suggested by electrostatic calculations (Figure 4C), but several uncharged residues, including Leu106, Gly107, Gly119, Ala118, Leu65, and Pro67 are localized to this region that would stabilize the hydrophobic phenyl ring of **2477**.

Our electrostatic surface map calculations suggest that the oxyanion holes of SpeB and staphopain A both are directly adjacent to the carbonyl and thus stabilize the molecule via a water molecule (Figure 4A,C). However, superposition of the papain structure onto SpeB shows that the papain oxyanion hole is not likely accessible by **2477**. Therefore, the weaker affinity of **2477** for papain in comparison to that of SpeB is likely due to the misalignment of the **2477** carbonyl with respect to the papain oxyanion hole. In all three proteases, the nitrile group is located in a moderately charged surface (Figure 4). The majority of interactions between SpeB and **2477** are through hydrogen bonding networks between the molecule and main-chain atoms, and these bonds are likely to be conserved in papain and staphopain A.

Our crystal structure of SpeB in complex with **2477** suggests that SpeB-specific small molecule inhibitors can be iteratively

DOI: 10.1021/acs.biochem.5b00607
Biochemistry 2015, 54, 4365−4373

designed to harness unique interactions with SpeB active site residues relative to other clan CA proteases. Exploiting unique SpeB electrostatic interactions would greatly improve the specificity and potency of **2477**. We analyzed the inhibitory capabilities of a range of **2477**-related compounds to determine the structure−activity relationship (SAR) between **2477** and SpeB through conducting kinetic assays to determine the IC_{50} values of each molecule. This provided clues about which portions of **2477** are important for SpeB inhibition and sheds light on modifications that can be made to impart the specificity of a small molecule for SpeB over other papain-like proteases.

On the basis of our crystal structure, we hypothesized that alterations to the backbone of **2477** would likely not be tolerated, as these moieties interact with main-chain atoms occluded within a narrow pocket of the SpeB active site. Lack of inhibition by compounds **1**−**6** verifies that the carbamate nitrogen and nitrile are necessary for effective SpeB and papain binding. Removal of these moieties from **2477** compromises the hydrogen bond network between the SpeB and papain active sites with the molecule, leaving the predominant interactions between **2477** and the proteases to nonspecific hydrophobic interactions. Compounds **2** and **3** conserve the carbamate and nitrile without adding steric bulk to the molecule, which would be spatially problematic for effective active site binding, as is likely the reason for poor inhibition by compounds **1**, **4**, and **5** (Figure 5 and Figures S4, S5, and S6, Supporting Information). Additionally, the increase in molecular hydrophobicity of the appended groups in **1**, **4**, and **5** likely disrupt several potential electrostatic and hydrogen bonding interactions that secure **2477** into the SpeB active site.

Slight inhibition of both SpeB and papain by **3** indicates that the phenyl ring of **2477** is preferred to the bulkier *tert*-butyl group. Although the hydrophobicity of this portion of the inhibitor is conserved, the spatial requirements for inhibition are made evident by the differential inhibition by **2477** and **3**. This is further supported by the greater inhibition of papain compared to that of SpeB, as this portion of the active site of papain is wider than that of SpeB (Figure 5). Compound **6** failed to inhibit both SpeB and papain, and the sole modification is the replacement of the nitrile of **2477** with an amine. This suggests that the rigidity of the triple bond in the nitrile of **2477** is essential to molecule binding and plays a larger role than the carbamate nitrogen in imparting specificity for papain-like proteases.

We also hypothesized that additions to the phenyl ring of **2477** could promote its inhibitory potency against SpeB. In particular, establishing an interaction between **2477** and SpeB residue Gln332 (which is not conserved in papain or staphopain A) may improve precision in this binding region that appears to be dominated by nonspecific, hydrophobic interactions. An addition of polarity in this area could be further stabilized by the coordination of a water molecule by **2477** and Ser391 (Figure 7).

Papain's active site is wider and therefore more conducive to various additions to the phenyl ring, as is evidenced by the effective inhibition by **7**−**11** (Figure 5C and Figure S8, Supporting Information). Compound **7** is much larger than **2477** and was less potent against SpeB than papain. Varying the position of the additions to the phenyl ring at the *ortho* (compounds **8** and **11**), *meta* (compound **8**), and *para* (compounds **9**, **10**, and **11**) positions did not obstruct the inhibitory potential of papain, while only the *ortho* and *meta*

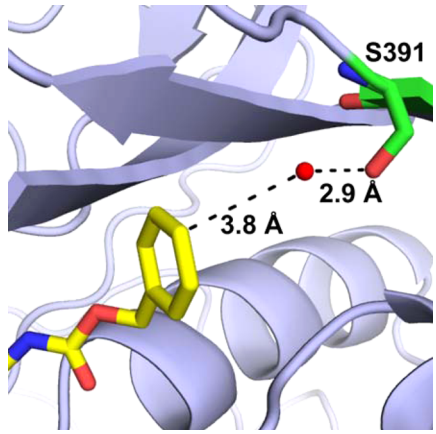

Figure 7. A potential interaction between **2477** and Ser391 can be exploited by modifying **2477**. Appending a polar group on the phenyl ring may add polarity to the molecule, allowing for stronger and more specific binding of **2477** to the SpeB active site. This interaction would be stabilized by a water molecule that coordinates active site residue Ser391.

modifications of **8** were tolerated by SpeB (Figure 5A,B and Figure S7, Supporting Information).

Furthermore, the electrostatic surface map of papain (Figure 4B) shows greater polarity than the corresponding portion of SpeB, with polar residues such as Ser131, Ser205, His159, and Asp158, allowing papain to accommodate polar additions to the phenyl ring of **2477** in a variety of positions (Figure 5C and Figure S8, Supporting Information). This portion of the SpeB active site is predominantly hydrophobic, although the nitro group on the phenyl ring of **8** may interact with Gln332 of SpeB, thus accounting for some inhibitory potential (Figure 5B and Figure S7, Supporting Information). Given the orientation of **2477** in the active site, polar substitutions in other positions on the phenyl ring would disrupt the hydrophobicity of the pocket as well as add steric bulk to a pocket that is narrow compared to that of papain. The differential effects of **7**−**11** on SpeB versus papain suggest that specificity for SpeB over other clan CA proteases may be achieved through modification of the phenyl ring of **2477**.

The broad substrate specificity of SpeB and other papain-fold cysteine proteases presents a significant challenge in the development of specific, active site-directed inhibitors. We present here a first-in-class small molecule that reversibly inhibits SpeB, and our X-ray crystal structure of the SpeB-**2477** complex and SAR studies provide insight into the iterative development of a more potent SpeB small molecule inhibitor.

■ ASSOCIATED CONTENT

Ⓢ Supporting Information

SpeB and papain activity with substrate Ac-AIK-AMC; K_i determination of **2477** with SpeB; K_i determination of **2477** with papain; structures of **2477**-related molecules **1**−**11**; IC_{50} assay of **1**−**6** against SpeB; IC_{50} assay of **1**−**6** against papain; IC_{50} assay of **7**−**11** against SpeB; and IC_{50} assay of **7**−**11** against papain. The Supporting Information is available free of charge on the ACS Publications website at DOI: 10.1021/acs.biochem.5b00607.

■ AUTHOR INFORMATION

Corresponding Author

*E-mail: wolan@scripps.edu.

DOI: 10.1021/acs.biochem.5b00607
Biochemistry 2015, 54, 4365−4373

Funding

The authors gratefully acknowledge financial support from The Scripps Research Institute and the National Science Foundation (to A.Y.W.).

Notes

The authors declare no competing financial interest.

■ ACKNOWLEDGMENTS

We thank Professor H. Rosen and Dr. S. Brown for access to HTS instrumentation, Drs. R. Stanfield and M. Elsliger for computational assistance, and the staff of the Stanford Synchrotron Radiation Lightsource.

■ ABBREVIATIONS

GAS, group A *streptococcus*; SAR, structure−activity relationship

■ REFERENCES

(1) Rawlings, N. D., Barrett, A. J., and Bateman, A. (2012) MEROPS: the database of proteolytic enzymes, their substrates and inhibitors. *Nucleic Acids Res. 40*, D343−350.

(2) Yu, C. E., and Ferretti, J. J. (1991) Frequency of the erythrogenic toxin B and C genes (speB and speC) among clinical isolates of group A *streptococci*. *Infect. Immun. 59*, 211−215.

(3) Musser, J. M., and DeLeo, F. R. (2005) Toward a genome-wide systems biology analysis of host-pathogen interactions in group A *Streptococcus*. *Am. J. Pathol. 167*, 1461−1472.

(4) Collin, M., and Olsen, A. (2001) EndoS, a novel secreted protein from *Streptococcus pyogenes* with endoglycosidase activity on human IgG. *EMBO J. 20*, 3046−3055.

(5) Kapur, V., Majesky, M. W., Li, L. L., Black, R. A., and Musser, J. M. (1993) Cleavage of interleukin 1β (IL-1β) precursor to produce active IL-1β by a conserved extracellular cysteine protease from *Streptococcus pyogenes*. *Proc. Natl. Acad. Sci. U. S. A. 90*, 7676−7680.

(6) Herwald, H., Collin, M., Muller-Esterl, W., and Bjorck, L. (1996) Streptococcal cysteine proteinase releases kinins: a virulence mechanism. *J. Exp. Med. 184*, 665−673.

(7) Sumitomo, T., Nakata, M., Higashino, M., Terao, Y., and Kawabata, S. (2013) Group A streptococcal cysteine protease cleaves epithelial junctions and contributes to bacterial translocation. *J. Biol. Chem. 288*, 13317−13324.

(8) Kapur, V., Topouzis, S., Majesky, M. W., Li, L. L., Hamrick, M. R., Hamill, R. J., Patti, J. M., and Musser, J. M. (1993) A conserved *Streptococcus pyogenes* extracellular cysteine protease cleaves human fibronectin and degrades vitronectin. *Microb. Pathog. 15*, 327−346.

(9) Berge, A., and Bjorck, L. (1995) Streptococcal cysteine proteinase releases biologically active fragments of streptococcal surface proteins. *J. Biol. Chem. 270*, 9862−9867.

(10) Connolly, K. L., Roberts, A. L., Holder, R. C., and Reid, S. D. (2011) Dispersal of Group A streptococcal biofilms by the cysteine protease SpeB leads to increased disease severity in a murine model. *PLoS One 6*, e18984.

(11) Connolly, K. L., Braden, A. K., Holder, R. C., and Reid, S. D. (2011) Srv mediated dispersal of streptococcal biofilms through SpeB is observed in CovRS+ strains. *PLoS One 6*, e28640.

(12) Walker, M. J., McArthur, J. D., McKay, F., and Ranson, M. (2005) Is plasminogen deployed as a *Streptococcus pyogenes* virulence factor? *Trends Microbiol. 13*, 308−313.

(13) Hollands, A., Gonzalez, D., Leire, E., Donald, C., Gallo, R. L., Sanderson-Smith, M., Dorrestein, P. C., and Nizet, V. (2012) A bacterial pathogen co-opts host plasmin to resist killing by cathelicidin antimicrobial peptides. *J. Biol. Chem. 287*, 40891−40897.

(14) Gotz, M. G., Caffrey, C. R., Hansell, E., McKerrow, J. H., and Powers, J. C. (2004) Peptidyl allyl sulfones: a new class of inhibitors for clan CA cysteine proteases. *Bioorg. Med. Chem. 12*, 5203−5211.

(15) Powers, J. C., Asgian, J. L., Ekici, O. D., and James, K. E. (2002) Irreversible inhibitors of serine, cysteine, and threonine proteases. *Chem. Rev. 102*, 4639−4750.

(16) Otto, H. H., and Schirmeister, T. (1997) Cysteine Proteases and Their Inhibitors. *Chem. Rev. 97*, 133−172.

(17) Greenbaum, D. C., Arnold, W. D., Lu, F., Hayrapetian, L., Baruch, A., Krumrine, J., Toba, S., Chehade, K., Bromme, D., Kuntz, I. D., and Bogyo, M. (2002) Small molecule affinity fingerprinting. A tool for enzyme family subclassification, target identification, and inhibitor design. *Chem. Biol. 9*, 1085−94.

(18) Thompson, L. A., and Ellman, J. A. (1996) Synthesis and Applications of Small Molecule Libraries. *Chem. Rev. 96*, 555−600.

(19) Wang, W., Jiang, J., Ballard, C. E., and Wang, B. (1999) Prodrug approaches to the improved delivery of peptide drugs. *Curr. Pharm. Des. 5*, 265−287.

(20) Gonzalez-Paez, G. E., and Wolan, D. W. (2012) Ultrahigh and high resolution structures and mutational analysis of monomeric *Streptococcus pyogenes* SpeB reveal a functional role for the glycine-rich C-terminal loop. *J. Biol. Chem. 287*, 24412−24426.

(21) Nomizu, M., Pietrzynski, G., Kato, T., Lachance, P., Menard, R., and Ziomek, E. (2001) Substrate specificity of the streptococcal cysteine protease. *J. Biol. Chem. 276*, 44551−44556.

(22) Vickers, C. J., Gonzalez-Paez, G. E., Litwin, K. M., Umotoy, J. C., Coutsias, E. A., and Wolan, D. W. (2014) Selective inhibition of initiator versus executioner caspases using small peptides containing unnatural amino acids. *ACS Chem. Biol. 9*, 2194−2198.

(23) Otwinowski, Z., and Minor, W. (1997) Processing of X-ray diffraction data collected in oscillation mode. *Meth. Enzymol. 276*, 307−326.

(24) McCoy, A. J., Grosse-Kunstleve, R. W., Adams, P. D., Winn, M. D., Storoni, L. C., and Read, R. J. (2007) Phaser crystallographic software. *J. Appl. Crystallogr. 40*, 658−674.

(25) Collaborative Computational Project, N. (1994) The CCP4 Suite: Programs for Protein Crystallography. *Acta Crystallogr., Sect. D: Biol. Crystallogr. 50*, 760−763.10.1107/S0907444994003112

(26) Emsley, P., Lohkamp, B., Scott, W. G., and Cowtan, K. (2010) Features and development of Coot. *Acta Crystallogr., Sect. D: Biol. Crystallogr. 66*, 486−501.

(27) Adams, P. D., Afonine, P. V., Bunkoczi, G., Chen, V. B., Davis, I. W., Echols, N., Headd, J. J., Hung, L. W., Kapral, G. J., Grosse-Kunstleve, R. W., McCoy, A. J., Moriarty, N. W., Oeffner, R., Read, R. J., Richardson, D. C., Richardson, J. S., Terwilliger, T. C., and Zwart, P. H. (2010) PHENIX: a comprehensive Python-based system for macromolecular structure solution. *Acta Crystallogr., Sect. D: Biol. Crystallogr. 66*, 213−221.

(28) Laskowski, R. A., MacArthur, M. W., Moss, D. S., and Thornton, J. M. (1993) PROCHECK: a program to check the stereochemical quality of protein structures. *J. Appl. Crystallogr. 26*, 283−291.

(29) Hooft, R. W., Vriend, G., Sander, C., and Abola, E. E. (1996) Errors in protein structures. *Nature 381*, 272.

(30) Chen, V. B., Arendall, W. B., 3rd, Headd, J. J., Keedy, D. A., Immormino, R. M., Kapral, G. J., Murray, L. W., Richardson, J. S., and Richardson, D. C. (2010) MolProbity: all-atom structure validation for macromolecular crystallography. *Acta Crystallogr., Sect. D: Biol. Crystallogr. 66*, 12−21.

(31) Berman, H. M., Westbrook, J., Feng, Z., Gilliland, G., Bhat, T. N., Weissig, H., Shindyalov, I. N., and Bourne, P. E. (2000) The Protein Data Bank. *Nucleic Acids Res. 28*, 235−242.

(32) Weiss, M. S., and Hilgenfeld, R. (1997) On the use of the merging R factor as a quality indicator for X-ray data. *J. Appl. Crystallogr. 30*, 203−205.

(33) Weiss, M. S. (2001) Global indicators of X-ray data quality. *J. Appl. Crystallogr. 34*, 130−135.

(34) Karplus, P. A., and Diederichs, K. (2012) Linking crystallographic model and data quality. *Science 336*, 1030−1033.

(35) Hofener, M., Pachl, F., Kuster, B., and Sewald, N. (2015) Inhibitor-based affinity probes for the investigation of JAK signaling pathways. *Proteomics*, n/a.

DOI: 10.1021/acs.biochem.5b00607
Biochemistry 2015, 54, 4365−4373

(36) Kamphuis, I. G., Kalk, K. H., Swarte, M. B., and Drenth, J. (1984) Structure of papain refined at 1.65 Å resolution. *J. Mol. Biol. 179*, 233−256.
(37) Hofmann, B., Schomburg, D., and Hecht, H. J. (1993) Crystal structure of a thiol proteinase from *Staphylococcus aureus* v-8 in the e-64 inhibitor complex. *Acta Crystallogr., Sect.A 49*, 102.

DOI: 10.1021/acs.biochem.5b00607
Biochemistry 2015, 54, 4365−4373